Gynecologic Oncology Reports 39 (2022) 100926

Contents lists available at ScienceDirect

Gynecologic Oncology Reports

journal homepage: www.elsevier.com/locate/gynor

Research Report

Understanding the impact of chemotherapy on the immune landscape of high-grade serous ovarian cancer

Rami Vanguri [a,1], Jamal Benhamida [b,1], Jonathan H. Young [c], Yanyun Li [b], Oliver Zivanovic [d], Dennis Chi [d], Alexandra Snyder [e], Travis J. Hollmann [b,f,2], Katherine L. Mager [g,*,2]

[a] Computational Oncology Service, Department of Epidemiology and Biostatistics, Memorial Sloan Kettering Cancer Center, New York, NY, USA
[b] Department of Pathology, Memorial Sloan Kettering Cancer Center, New York, NY, USA
[c] School of Medicine, Texas Tech University Health Sciences Center, Lubbock, TX, USA
[d] Gynecology Service, Department of Surgery, Memorial Sloan Kettering Cancer Center, New York, NY, USA
[e] Department of Medicine, Memorial Sloan Kettering Cancer Center, New York, NY, USA
[f] Parker Institute for Cancer Immunotherapy, Memorial Sloan Kettering Cancer Center, New York, NY, USA
[g] Department of Gynecologic Oncology, Roswell Park Comprehensive Cancer Center, Buffalo, NY, USA

ARTICLE INFO

Keywords:
Ovarian cancer
Tumor microenvironment
Immunotherapy

ABSTRACT

Objectives: We quantitatively characterized the change in temporospatial expression of repressive and stimulatory checkpoints across immune cell populations in the tumor microenvironment in a cohort of high grade serous ovarian carcinomas (HGSOC) using matched samples before and after neoadjuvant platinum-based chemotherapy.

Methods: Using retrospectively collected matched tissue samples from 9 patients, cell populations were assessed using multiplex immunofluorescence using the Vectra Multispectral Imaging System (Perkin Elmer). We used multiple panels to assess: tumor (AE1/AE3), T cells (CD3, CD8, FOXP3), macrophages (CD68) as well as immune checkpoints (C3aR, PD-1, PD-L1, LAG3, IDO, ICOS, GITR). IHC staining was performed for folate receptor status. Changes in immune cell populations as well as intensities of associated repressive and stimulatory proteins were assessed pre- to post-treatment.

Results: We observed a consistently high pre-treatment stromal macrophage population which is reduced post-chemotherapy with post-treatment enrichment in macrophage PD-L1 expression. While inhibitory checkpoint expression on T cells was heterogeneous post-chemotherapy, we observed a change in the T_hICOS+:T_{reg} ratio which resulted in T_hICOS+ cells outnumbering T_{reg} cells post-treatment. Spatial analysis revealed the proximity of T_{reg} cells to T_hICOS+ T cells decreased post-treatment. We also observed upward shifts in T_{eff}:T_{reg} T cell ratios with retention of immune checkpoints PD-1, LAG3 and GITR.

Conclusions: In this unique dataset of pre and post matched chemotherapy treated HGSOC patients, we observed changes in immune cell subsets expressing repressive or stimulatory proteins resulting in immune compositions more favorable to checkpoint modulations, suggesting novel therapeutic strategies in the recurrent setting.

1. Introduction

High-grade serous ovarian cancer (HGSOC) is characterized by high response rates to initial treatment with either neoadjuvant chemotherapy (NACT) or primary debulking with adjuvant chemotherapy followed by high rates of recurrence and development of resistance to standard therapy (Bowtell et al., 2015). Despite advances in surgical technique and systemic treatments, ovarian cancer remains the fifth leading cause of cancer related death in women. Novel agents are needed to continue making progress in treating this complex disease.

Immunotherapy has shown promise in some gynecologic cancers, such as the combination of pembrolizumab and lenvatinib, with a response rate of 37% (Makker et al., 2019), prompting accelerated approval by the FDA (Center for Drug Evaluation, Research, 2019).

* Corresponding authors at: Roswell Park Comprehensive Cancer Center, Elm and Carlton Streets, Buffalo, NY 14263, USA.
E-mail address: Katherine.LaVigneMager@roswellpark.org (K.L. Mager).
[1] These authors contributed equally: Rami Vanguri, Jamal Benhamida.
[2] These authors contributed equally: Travis J. Hollmann, Katherine L. Mager.

https://doi.org/10.1016/j.gore.2022.100926
Received 21 September 2021; Received in revised form 7 December 2021; Accepted 3 January 2022
Available online 7 January 2022

Unfortunately, the use of single agent immunotherapy in ovarian cancer has not yet shown the same success, with the best published response rates of 15% (Varga et al., 2015; Hamanishi et al., 2015) in heavily pretreated patients. However, among patients who do respond, the response is frequently durable (Zamarin et al., 2020).

There is a growing literature on the tumor immune microenvironment (TME) in HGSOC, with most work done in the treatment naïve setting (Zhang et al., 2003). Multiple studies that examined untreated tissue samples have shown a prognostic effect for tumor infiltrating lymphocytes (TILs) and immune gene expression signatures (Ovarian Tumor Tissue Analysis (OTTA) Consortium, 2017; Verhaak et al., 2013), implying the presence of a substrate for checkpoint blockade activity in some patients. A better understanding of the effect of NACT on the TME could aid in the development of more effective regimens through treatment timing, patient selection, combination therapies or novel. Adding to the complexity of the TME in ovarian cancer, prior work has shown significant intra-patient heterogeneity in immune composition (Jiménez-Sánchez et al., 2020) and checkpoint expression (Blanc-Durand et al., 2021).

We utilized multiplex immunofluorescence to investigate pre-post expression changes of immune checkpoints on T cells and macrophages including: programmed cell death protein 1 (PD-1), programmed death-ligand 1 (PD-L1), lymphocyte-activation gene-3 (LAG3), inducible T-cell costimulator (ICOS), glucocorticoid-induced TNFR-related protein (GITR), indoleamine 2,3-dioxygenase (IDO) and complement component 3a receptor 1 (C3aR). PD-1 expression on T_{eff} cells induces exhaustion resulting in loss of effector function (Barber et al., 2006). PD-L1, a ligand to PD-1, is expressed on tumor and antigen presenting cells including macrophages. PD-L1 binds to PD-1 resulting in immune tolerance. LAG3 also suppresses T cell activation. GITR is expressed T_{reg}, T_h and T_{eff} cells and expression increases with activation. While overall immune activating, GITR can have a suppressive effect through T_{reg} activation (Shevach and Stephens, 2006). ICOS expression on T cells plays a role in regulating adaptive T cell response which can be both anti-tumor through T cell activation as well as suppressive through the increase of T_{reg} cells. IDO modulates inflammation and is correlated with reduced T-cell mediated response in model systems (Mellor and Munn, 2004). C3aR is expressed on myeloid cells including macrophages and was shown in animal studies to regulate T cell mediated antitumor immunity (Martin et al., 1997; Wang et al., 2019 Jul).

In this study we aimed to evaluate the effect of NACT on the expression and spatial distributions of immune checkpoints using paired tissue samples before and after therapy including a subset of site-matched samples. Specifically, we evaluated changes in expression of inhibitory checkpoints PD-1 and LAG3 on T_{eff} cells after NACT. Stimulatory checkpoints GITR and ICOS were evaluated on T_{eff} and T_h cells, respectively. We also assessed changes in checkpoint expression of populations that promote immune activation relative to suppressive populations including PD-1+T_{eff}:T_{reg}, LAG3+T_{eff}:T_{reg}, ICOS+T_h:T_{reg} and GITR+T_{eff}:T_{reg}. Finally, we assessed pre-post changes in the proportion of macrophages expressing inhibitory checkpoints PD-L1, IDO and C3aR.

2. Materials and methods

2.1. Cohort characteristics and selection of specimens

48 paired tumors were identified after review of all patients with HGSOC from an institutional database that included patients treated in the standard-of-care setting between 2008 and 2013 and had tissue samples available before and after treatment. Nine of these patients had adequate residual tumor present in paired tissue samples prior to NACT and at interval debulking surgery to perform multiplex immunofluorescence. All samples were obtained from formalin-fixed paraffin embedded blocks.

Patient characteristics are listed in Table 1. Five patients' pre- and post-therapy samples were collected from the same anatomic site (site-matched cases). All patients were diagnosed with stage IIIC or IV HGSOC and all received NACT with carboplatin and a taxane (either paclitaxel or docetaxel) with a median of 4 cycles (range 3–6). Two patients (22%) had germline mutations in BRCA captured in the course of routine clinical care. Somatic BRCA status was not assessed during this study. There was not sufficient tissue to perform on the remaining available specimens and molecular testing was not routinely being obtained for clinical care during the period patients were being treated.

2.2. Seven-color immunohistochemical multiplex staining

We performed three multiplex immunofluorescence assays to characterize the TME before and after treatment in order to assess T cell exhaustion (CD8, FOXP3, Ki-67, PD-1, LAG3), regulatory T cells (CD3, CD8, FOXP3, GITR, ICOS) and macrophages (CD68, CD3, C3aR, PD-L1, IDO). All panels included a tumor marker (AE1/AE3). 4 um sections obtained from tissue blocks were baked for 2 h at 62 degrees with deparaffinization performed on the Leica Bond RX followed by six sequential rounds of staining, each round including a combined block with primary antibody (PerkinElmer antibody diluent/block ARD1001) followed by a corresponding secondary horseradish peroxidase (HRP)-conjugated polymer (PerkinElmer Opal polymer HRP Ms + Rb ARH1001). Each HRP-conjugated polymer induces the covalent binding

Table 1
Patient characteristics.

Subject ID	Age	BRCA status	Stage	Type of Chemo	Number of Cycles	Platinum Sensitive	Site Matched	Progression Free Survival (Months)	Overall Survival (Months)	Status
2359	68	Negative	IIIC	Carbo/ paclitaxel	6	N	Y	17.4	46	DOD
0564	73	Negative	IV	Carbo/ paclitaxel	6	N	Y	15.5	38	DOD
6965	45	BRCA1	IIIC	Carbo/ docetaxel	4	Y	Y	13	25	DOD
9347	60	Negative	IIIC	Carbo/ paclitaxel	3	Y	Y	12.1	51	DOD
7626	67	Negative	IIIC	Carbo/ paclitaxel	4	N	Y	7.2	49	AWD
7858	70	Negative	IIIC	Carbo/ paclitaxel	3	Y	N	6.5	39.5	DOD
6229	58	Negative	IV	Carbo/ paclitaxel	4	Y	N	13.2	39.6	AWD
6986	50	BRCA1	IV	Carbo/ docetaxel	5	N	N	18.4	27.7	DOD
2220	59	Negative	IV	Carbo/ docetaxel	3	N	N	5.5	7.5	DOD

of fluorophores using tyramide signal amplification. The covalent reaction was followed by heat induced stripping of the primary antibody in citric acid buffer (pH 6.0; Leica ER1) for 20 min at 100 degrees before the next step in the sequence. For each of the three staining panels, the six antibodies were sequentially stained and then were stained with Spectral DAPI (Perkin Elmer) to visualize nuclei and mounted with ProLong Gold antifade reagent mounting medium (Invitrogen).

2.3. Immunohistochemical staining

The FOLR1 primary antibody (Abcam, ab221543, EPR20277) was used at a concentration of 1.07 ug/ml for IHC staining. Immunohistochemical staining for FOLR1 was performed on 4-μm thick FFPE serial sections using an automated staining system (Leica Bond). Antigen retrieval was conducted for 30 min using Bond epitope retrieval solution 2 (EDTA, pH 9.0) followed by incubation of the primary antibody for 30 min. Appropriate positive controls were included in each staining run.

2.4. Multispectral imaging, spectral unmixing and cell segmentation

Seven color multiplex stained slides were imaged using the Vectra Multispectral Imaging System version 3 (Perkin Elmer). Scanning was performed at 20X. Filter cubes used for multispectral imaging were DAPI, FITC, Cy3, Texas Red and Cy5. A spectral library containing the emitted spectral peaks of the fluorophores in this study was created using the Vectra image analysis software (Perkin Elmer). Using multispectral images from single-stained slides for each marker, the library was used to separate each multispectral cube into individual components (spectral unmixing) allowing for identification of all seven marker channels of interest using inform 2.2.1 image analysis software. Images were exported to Indica Labs Halo image analysis platform. Cell segmentation and signal thresholding were performed separately on each case using a supervised proprietary segmentation algorithm and random forest classifier for tumor and stromal identification.

2.5. Statistics

We used the lifelines python package (Davidson-Pilon, 2021) to perform univariate Cox proportional hazard modeling. The significance of intensity changes from pre- to post-treatment were assessed with a *t*-test, using the distributions of intensities above the threshold to be considered positive for the marker for a specific cell population, for each patient. For example, to calculate the significance in the change of macrophage PD-L1 intensity, the distributions of PD-L1 intensities in CD68+PD-L1+ cells before and after therapy are compared. Confidence levels on phenotypic ratios were assessed using standard error propagation from the original cell counts.

The hierarchical clustering analysis was performed using densities, reported as cell counts per unit area stratified to stromal and tumor compartments. Differences between pre-treatment and post-treatment densities (cell count per mm^2) were calculated and L^2 normalized for each immune marker. Hierarchical clustering was performed on the density differences using Euclidean distance and average linkage. Only immune phenotypes with sufficiently high variance above a preset threshold across cases were retained for hierarchical clustering. Separately, for tumor or stroma compartments only, hierarchical clustering was performed on density counts in both before and after treatment. Heatmaps for these density counts show values transformed by $\log(p + 1)$, where p is the density count. All clustering analyses were implemented in R with the pheatmap library. Additionally, we study the intensity of targetable markers (C3aR, PD-L1, IDO, PD-1, LAG3, GITR and ICOS) and their differences from pre-treatment to post-treatment.

3. Results

3.1. Baseline immune characteristics of the untreated tumor microenvironment were patient specific

Baseline immune characteristics of the tumor microenvironment (TME) before and after treatment are shown in Fig. 1. Prior to chemotherapy, CD68+ macrophages represented the most consistently abundant cell type in both the tumor and stromal compartments before treatment (Fig. 1). CD8+ (T_{eff}), CD3+CD8-FOXP3 (T_h) and FOXP3+ (T_{reg}) cells were present in all patients in the pretreatment stromal compartment with significant heterogeneity across the cohort (Fig. 1C). Far fewer immune cells were seen in the pretreatment tumor compartment (Fig. 1A and B).

3.2. Post-treatment C3aR expressing macrophage density is associated with progression-free survival

We performed univariate Cox proportional hazard modeling of PFS using pre-treatment and post-treatment stromal cell densities including: CD68+ macrophages, T_{eff}, T_h, and T_{reg}. We also modeled checkpoint expressing pre-treatment and post-treatment stromal densities including: PD-L1+, IDO+ and C3aR+ on macrophages, PD1+, LAG3+ and GITR+ on T_{eff} and ICOS+ on T_h. In addition to the densities, we modeled pre-treatment and post-treatment checkpoint expression intensities. Only post-treatment stromal C3aR+CD68+ macrophages were found to be a significant predictor of PFS (HR = 6.1e-10, 95% CI 7.5e-19–0.5).

3.3. NACT induced changes in checkpoint expression density and intensity

We evaluated changes in checkpoint expressing immune cells after NACT. Changes were only evaluated on stromal populations due to the low number of intratumoral immune cells observed.

3.3.1. PD-L1, C3aR and IDO on macrophages and tumor

We observed macrophages to be the most abundant cell type within the pretreatment TME with large variance of PD-L1 expression before and after therapy (Fig. 2a). There was an enrichment in PD-L1+ stromal macrophages in 5/9 patients from pre to post treatment. Additionally, there was a significant change in the intensity of PD-L1 expressing stromal macrophages in 5/9 patients with an increase in 4 and decrease in 1. Significant changes in C3aR intensity on macrophages after treatment were observed in 6/9 patients (increase in 2, decrease in 4). C3aR macrophage expression was heavily enriched in case 2359 from 3% to 70% after treatment (Fig. 2b). No significant changes in stromal IDO expression were observed.

3.3.2. PD-1 and LAG3 on T_{eff}

There was a significant decrease in PD-1 intensity on T_{eff} cells in 2 cases and no significant change in the remaining cases (Fig. 3a). We observed higher PD-1+T_{eff}:T_{reg} ratios after therapy in 4/9 patients and decreases in the remaining patients. Case 6986 PD-1+T_{eff}:T_{reg} exhibited a large increase from 0.06 to 0.42 after therapy. Case 6229 did not exhibit a change in PD-1+T_{eff}:T_{reg} after treatment, but was the only case where PD-1+T_{eff} cells consistently outnumbered T_{reg} cells after treatment. Significant decreases in PD-1 intensity on T_{eff} cells were observed in 2 cases. LAG3 expression was heterogeneous in both the tumor and stroma on T_{reg} cells. Similar to PD-1, we observed increases in the LAG3+T_{eff}:T_{reg} in 5/9 patients, decreases in 3 cases (Fig. 3) and a depletion of LAG3 expressing T_{eff} cells in case 2359. No significant change in LAG3 intensity on T_{eff} cells was observed.

Increases of T_{eff}:T_{reg} ratios with retention of both PD-1 and LAG3 on T_{eff} cells was observed in 4/9 patients. Both the LAG3+T_{eff}:T_{reg} and PD-1+T_{eff}:T_{reg} ratios remained below 1 after therapy, indicating a greater

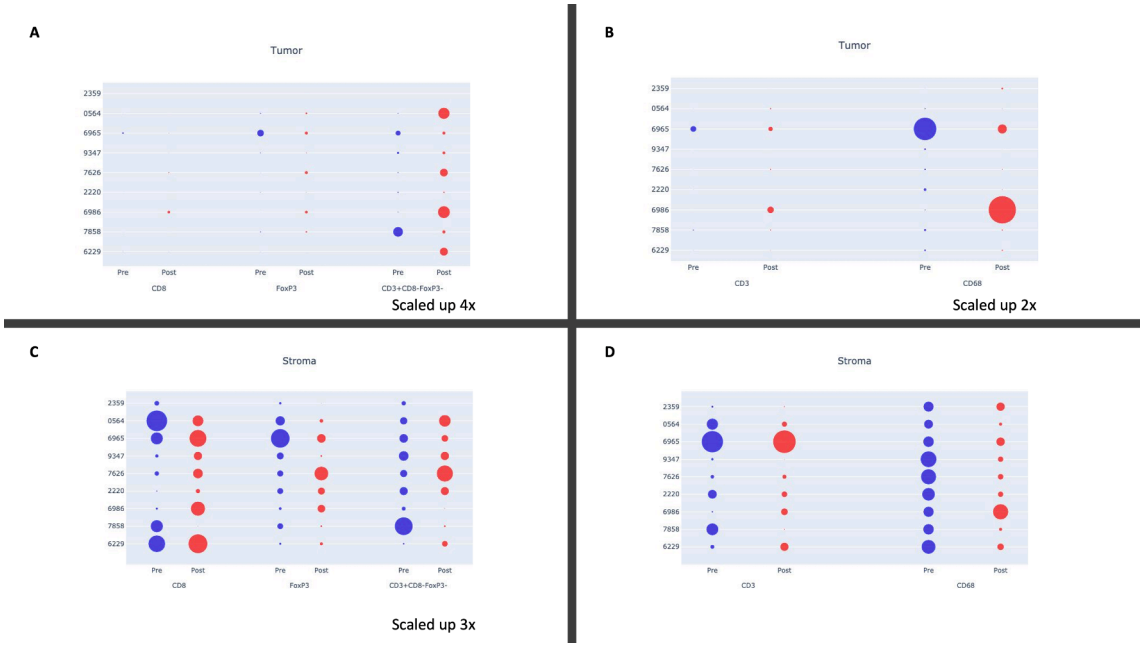

Fig. 1. Immune cell populations before and after treatment with NACT, stratified by the tumor (a,c) and stromal (b,d) compartments. To increase visibility, small cell populations were stratified and scaled up. Effector (CD8+), regulatory (FOXP3+) and helper (CD3+CD8-FOXP3-) (a,c) T-cells are shown separately from overall T-cell (CD3+) and macrophage (CD68+) populations to enhance visual comparison.

abundance of T_{reg} cells relative to checkpoint expressing T_{eff} cells. The remaining patient, case 6229, exhibited no change in the PD-1+T_{eff}:T_{reg} ratio from pre to post.

3.3.3. *ICOS on T_h and GITR on T_{eff}*

There was a decrease of ICOS expressing CD8+ T cells in 7/9 patients. There was a significant increase of ICOS intensity on T_h cells in 3 cases and decrease in 2 (Fig. 4a). We observed increases in the T_hICOS+:T_{reg} in 6/9 patients. In 4 of these patients, the shift in T_hICOS+:T_{reg} corresponded to a selective retention of T_hICOS+ and elimination of T_{reg} cells, resulting in the T_hICOS+ T cells outnumbering T_{reg} cells. Proximity analysis revealed significant decreases of T_{reg} cells in the vicinity (30 μm) of T_hICOS+ T cells in 5/9 patients (Fig. 4b).

We observed heterogeneous changes in GITR expression on T_{reg} cells after therapy. A significant decrease in GITR intensity on T_{eff} cells was observed in Case 6986 (Fig. 4c). An increase GITR+T_{eff}:T_{reg} was observed in 5/9 patients. Despite these increases, GITR+T_{eff}:T_{reg} ratios remained significantly below 1, indicating the relative abundance of T_{reg} cells compared to GITR+ T_{eff} cells after therapy. There were no GITR+ T_{eff} cells in case 2359 after treatment.

3.4. *Hierarchical clustering showed treatment driven changes in receptor expression*

We performed hierarchical clustering on stromal densities of all possible phenotypic combinations (Fig. 5a). The result showed the 2 patients with deleterious germline BRCA mutations (both BRCA1) demonstrate increased PD-L1+ expression following NACT. Many immune phenotype populations including ICOS+ (across all T cell types), IDO+, GITR+, CD8+PD-1+, CD8+LAG3+, and CD8+Ki-67+ exhibited low variance across all cases and thus little to no change in stromal densities between pre- and post- treatment. The CD68+ (both PD-L1+ and PD-L1-) macrophage stromal densities increased after treatment primarily in patients with the BRCA mutations while decreasing in all other cases. The FOXP3+ T cell stromal density increased post-treatment only in case 7626 while remaining relatively unchanged in all others. In contrast, the stromal CD8+ density increased in 6/9 patients. Clustering revealed the majority of these CD8+ T cells lack Ki-67 as well as the checkpoint inhibitors LAG3 and PD-1.

3.5. *Folate receptor expression did not correlate with baseline or changes in immune populations*

Folate receptors are tumor associated antigens that are frequently expressed in ovarian cancer, with overexpression noted on 70–90% of ovarian cancers (Kalli et al., 2008) and minimal expression on normal tissues. It has been targeted through the use of farletuzumab, a monoclonal antibody against folate receptor alpha, as well as through the use of folate receptor vaccines in conjunction with checkpoint blockade (Zamarin et al., 2020). It is also being targeted using an antibody drug conjugate, mirvetuximab. Initial data has been mixed (O'Malley et al., 2020; Moore et al., 2021 Jun), but trials are ongoing. We hypothesized that folate receptor expression would correlate with immune infiltrate. Overexpression was noted in 6/9 cases (67%). We did not observe consistent changes in folate expression after treatment, nor did we identify any correlation with changes in the TME (Fig. 5a and Supplementary Fig. 1). We also did not observe any correlation between folate expression and baseline immune composition in either the stroma or intratumorally (Supplementary Figs. 2 and 3).

4. Discussion

A better understanding of the TME in ovarian cancer would allow for new approaches to treatment and better utilization of immunotherapy in this disease. Most patients are treated with a first line regimen that combines surgery with a standard chemotherapy regimen of carboplatin and a taxane, but little is known about the effect on the TME. The majority of immunotherapy clinical trials have to date been conducted in heavily pretreated patients, although recent trials are beginning to look at its use in the upfront treatment setting. Unfortunately, these have not yet shown improved response over standard treatment (e.g., JAVELIN 100 (Ledermann et al., 2020).

In this study we performed multiplex staining on paired samples from a retrospective single-center cohort of 9 patients with ovarian cancer who had undergone NACT with carboplatin and taxanes to characterize the TME before and after treatment. We observed that

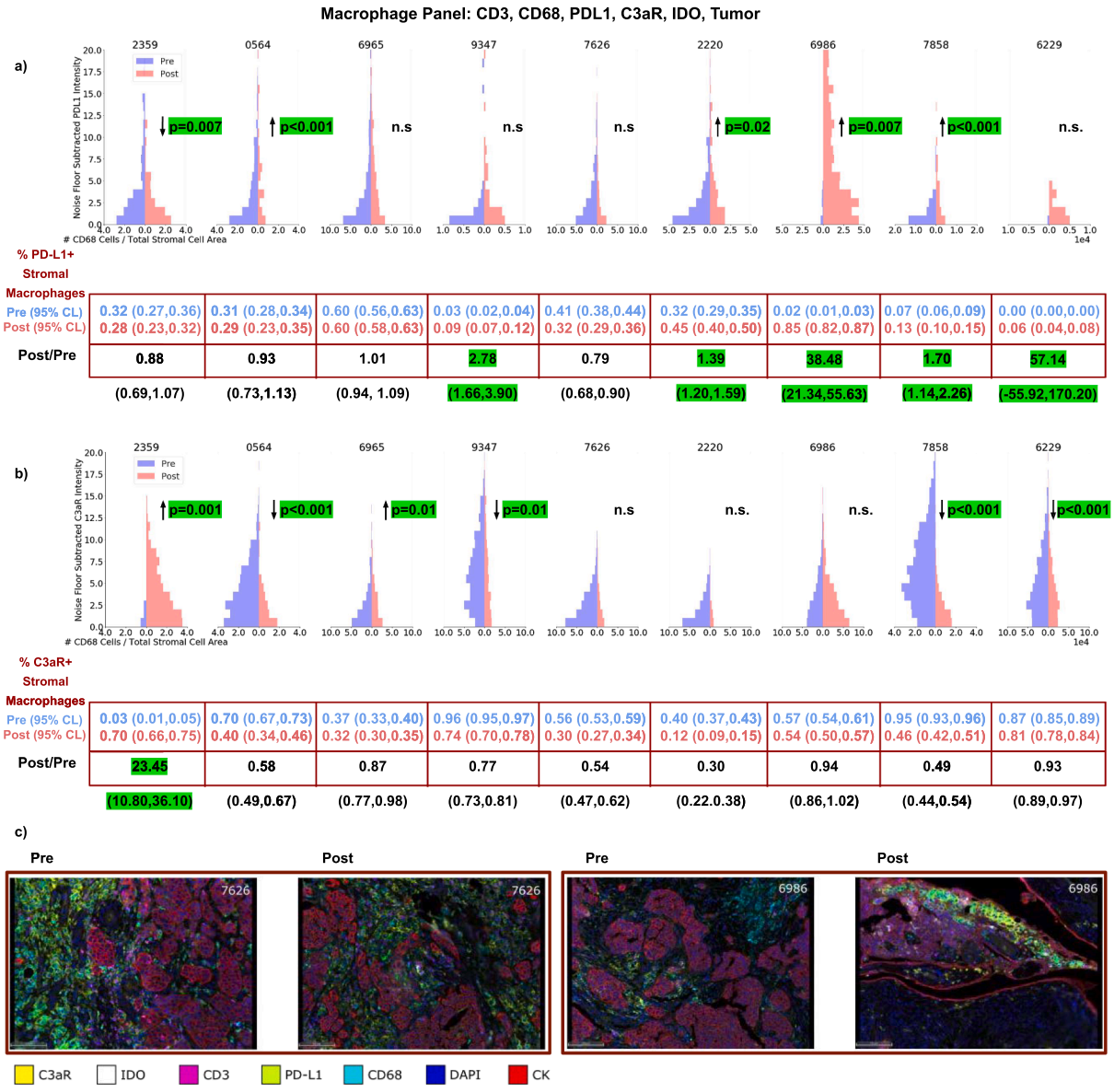

Fig. 2. Changes in the intensity of PD-L1 (a) and C3aR (b) expression on macrophages before and after NACT for each patient. Also shown are the changes in densities of macrophages expressing PD-L1 (a) and C3aR (b) after therapy. (c) Representative fields of view are shown for cases 7626 and 6986.

chemotherapy does not cause uniform change in immune cell populations overall, but did cause changes in subsets of markers and in specific subsets of patients (Fig. 5b). We did not observe effects specific to the sites being matched.

The largest component of the stromal cellular infiltrate before and after treatment was CD68+ macrophages (18%–30% of all detected stromal nuclei), which has been previously reported in ovarian cancer (Nowak et al., 2020 May). We observed consistent macrophage infiltration before and after treatment, suggesting macrophage targeting as a novel therapeutic strategy for either initial treatment or in the recurrent setting (Duan and Luo, 2021). Increased PD-L1 expression on macrophages after chemotherapy in 5/9 patients also suggests the usage of PD-L1 inhibitors in the recurrent setting, which have been observed to induce M1 repolarization (Sun et al., 2019; Gubin et al., 2018). C3aR was expressed on macrophages prior to treatment in all 9 patients and was retained in all patients after treatment, although reduced (Fig. 2b). We found post-treatment C3aR expressing macrophages were also found to be associated with progression-free survival using Cox proportional hazard modeling. However, this observation should be considered exploratory due to the size of the cohort. If confirmed in larger studies, modulation of C3aR could also be a novel therapeutic target in the initial or recurrent setting.

Stromal T cell infiltration was considerably smaller than macrophages: T_h (1%–11%), T_{eff} (3%–14%) and T_{reg} (2%–12%). While there was no clear trend of increase or decrease in ICOS expression on T_h cells after treatment (4 cases decrease, 5 increase), ICOS+T_h:T_{reg} ratios were more consistent. ICOS+T_h cells were preferentially retained over T_{reg} cells in 6/9 cases. In 4 of these 6 patients, the T_{reg} cells were outnumbered by the ICOS+T_h cells. Spatial analysis showed fewer T_{reg} cells in proximity of ICOS+T_h cells after treatment. These observations suggest ICOS agonism as a novel therapeutic target in HGSOC. The balance of GITR+T_{eff}:T_{reg} also increased in 5 cases, although the change was smaller than ICOS+T_h:T_{reg}.

We observed that T cells do not uniformly express high levels of exhaustion markers after treatment. However, in 4/9 patients, PD-1+ T_{eff} cells were preferentially retained over T_{reg} cells after treatment. Similarly, LAG3+ T_{eff} cells were preferentially retained in 5/9 patients after treatment. These findings suggest that a subset of patients may

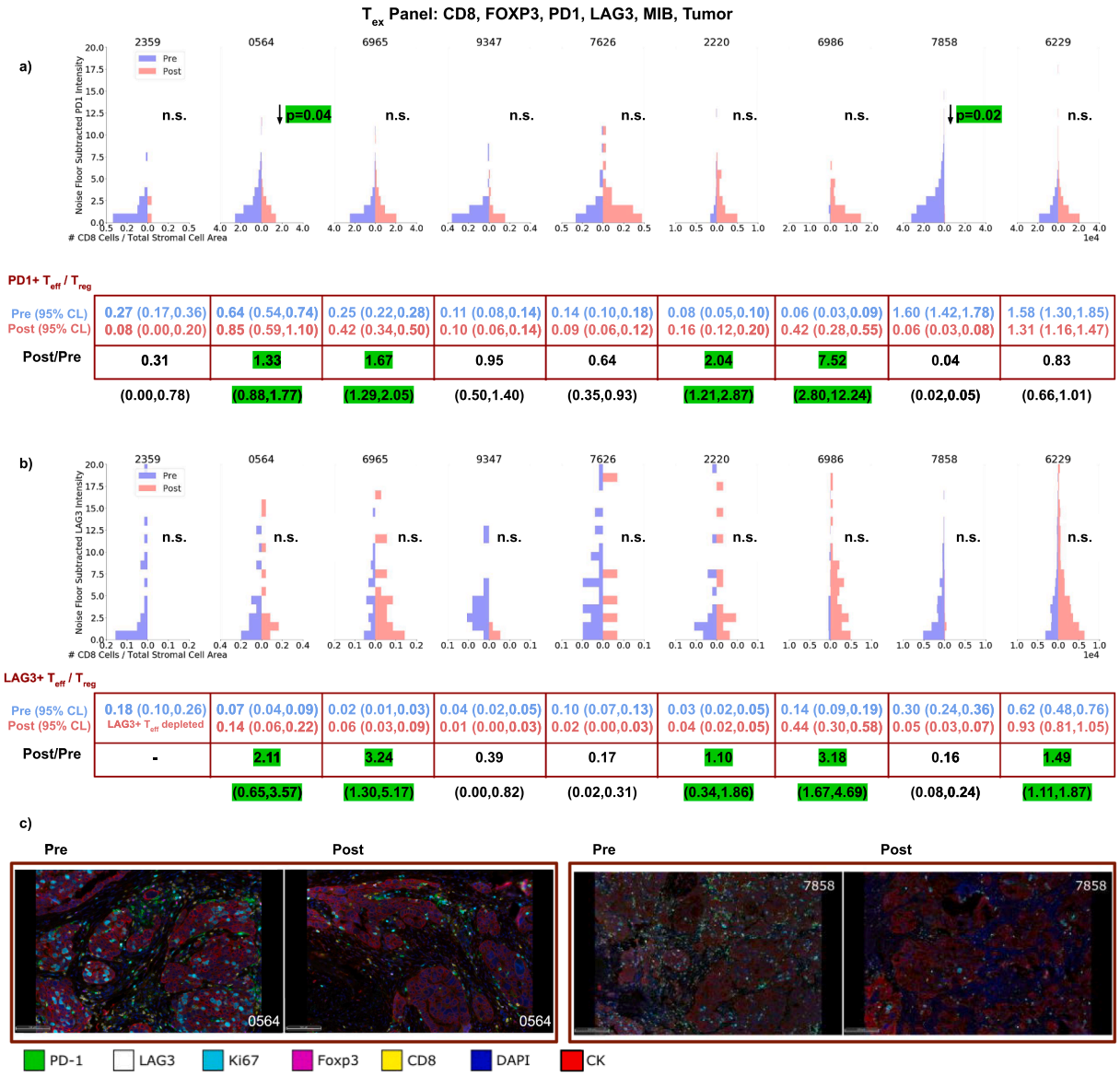

Fig. 3. Changes in the intensity of PD-1 (a) and LAG3 (b) expression on T_{eff} before and after NACT for each patient. Also shown are the changes in PD-1+T_{eff}:T_{reg} (a) and LAG3+T_{eff}:T_{reg} (b) after therapy. (c) Represenative fields of view are shown for cases 0564 and 7858.

benefit from checkpoint blockade targeting PD-1, PD-L1 or LAG3. However, these may not be the most effective agents for broad use if this dataset is representative of the HGSOC TME landscape. Additionally, hierarchical clustering showed increases in PD-L1 expression among the two germline BRCA+ patients following chemotherapy, which if replicated in a larger data set, could provide a rationale for checkpoint blockade at the time of treatment within this population.

We did not observe a significant trend towards either immune activation or suppression, However, case 6986 exhibited a more immune-activated phenotype. IHC markers in case 6986 suggested an adaptive immune response (T_{eff} cells) coupled with a compensatory suppressive markers (LAG3+ T_{eff} cells, C3aR+ and PD-L1+ macrophages) in tumor and stroma prior to treatment, which intensified after chemotherapy. Case 6986 also had the highest progression-free survival in our cohort (18.4 months). Due to the size of our cohort, this case is merely anecdotal. However, if the case is representative of a small subpopulation, this phenotype might represent an opportunity for patient-tailored therapy. Retrospective analyses of failed all-comers clinical trials would represent a first step towards determining if this case represents a small but consistent phenotype.

Prior studies have looked at the effect of NACT with carboplatin and paclitaxel on the immune profile of HGSOC, but this study utilized a broader panel that includes both T cell and macrophage populations as well as additional markers. Prior work has shown the significant impact that tumor heterogeneity has on the immune environment both between patients and between anatomic sites in the same patient (Brunekreeft et al., 2020). This work was primarily done by looking at gene expression, but more limited data is available on tissue level expression. Additionally, the data available includes much more limited marker panels (Mesnage et al., 2017). A recent study characterized IHC expression of PD-L1, IDO, LAG3 and TIM3 before and after NACT within an ovarian cancer cohort (Blanc-Durand et al., 2021). The study described an increase in PD-L1 and LAG3 expression following NACT overall, but a heterogeneous response was seen in site matched pairs in the majority of paired specimens. Our study adds to a better understanding of the effect of NACT at the protein level because of the depth of markers studied, a cohort that includes site matched pairs, and the ability to assess the temporospatial relationship of the immune infiltrate

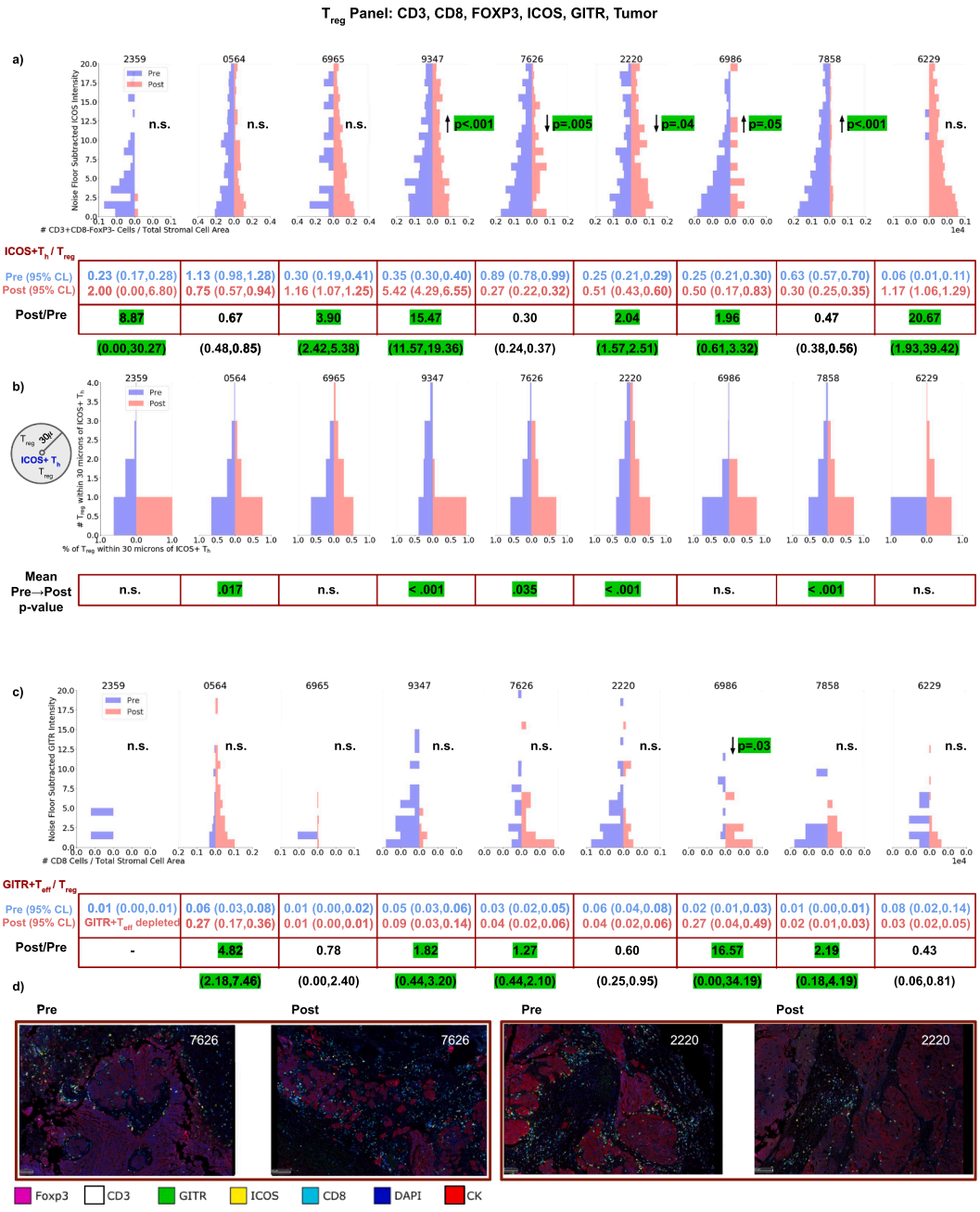

Fig. 4. Changes in the intensity of ICOS (a) expression on T_h for each patient as well as the spatial distribution changes of T_{reg} within 30 μm of ICOS+T_h (b) before and after NACT. Changes in the intensity of GITR (c) expression on T_{eff} before and after NACT is also shown. Also shown are changes in ICOS+T_h:T_{reg} (a) and GITR+T_{eff}:T_{reg} after therapy. (c) Representative fields of view are shown for cases 7626 and 2220.

using a multiplex imaging approach.

While this study is limited by a small sample size, subsets of patients exhibited changes in their immune composition that may be favorable to novel therapies including checkpoint modulation. This patient cohort was investigated in another study, which looked at changes seen on the RNA and TCR level but did not address protein-level expression (Jiménez-Sánchez et al., 2020). In addition, while the multiplexed assessment of immune cells at the protein-level represents an important step forward in understanding chemotherapy-treated HGSOC, such an analysis does not directly describe the functional characteristics of those cells. As such, this study was hypothesis-generating and requires examination within a larger cohort.

Study approval

The study was reviewed and approved by the Memorial Sloan Kettering institutional review board (New York, USA) under protocol 15-189. This was a waiver that allowed for the use of previously collected specimens under institutional tissue procurement protocols.

Funding

Research reported in this publication was supported in part by the National Cancer Institute of the National Institutes of Health under Award Number R25CA020449.

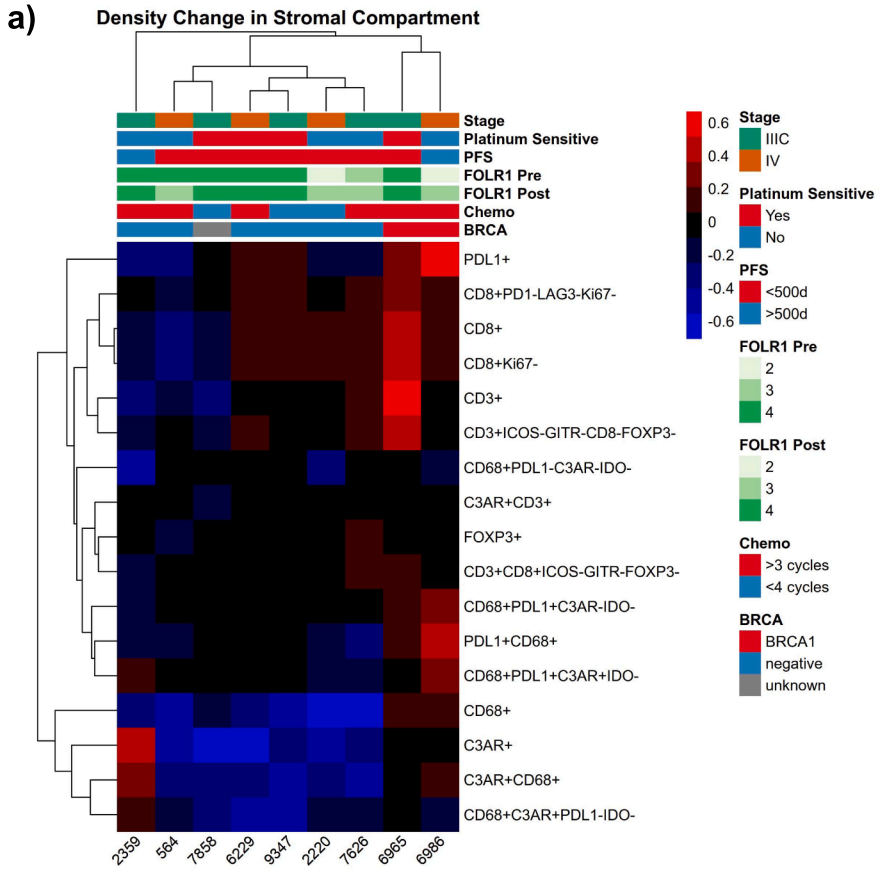

b) Density Change on Functional Cell Populations

	2359	0564	6965	9347	7626	2220	6986	7858	6229
CD68+PD-L1+	0.88	0.93	**1.01**	**2.78**	0.79	**1.39**	**38.48**	**1.70**	**57.14**
CD68+C3aR+	**23.45**	0.58	0.87	0.77	0.54	0.30	0.94	0.49	0.93
PD1+CD8+/FOXP3+	0.31	**1.33**	**1.67**	0.95	0.64	**2.04**	**7.52**	0.04	0.83
LAG3+CD8+/FOXP3+	-	**2.11**	**3.24**	0.39	0.17	**1.10**	**3.18**	0.16	**1.49**
ICOS+T_h/FOXP3+	**8.87**	0.67	**3.90**	**15.47**	0.30	**2.04**	**1.96**	0.47	**20.67**
GITR+CD8+/FOXP3+	-	**4.82**	0.78	**1.82**	**1.27**	0.60	**16.57**	**2.19**	0.43

Fig. 5. (a) Hierarchical clustering analysis was performed on changes in stromal densities before and after treatment. Populations with low variance across the cohort are not shown. (b) Summary of density changes on cell populations after therapy for each patient.

CRediT authorship contribution statement

Rami Vanguri: Formal analysis, Software, Validation, Visualization, Writing – original draft, Writing – review & editing. **Jamal Benhamida:** Formal analysis, Software, Validation, Visualization, Writing – original draft, Writing – review & editing. **Jonathan H. Young:** Formal analysis, Software, Writing – review & editing. **Yanyun Li:** Formal analysis, Project administration. **Oliver Zivanovic:** Resources, Writing – review & editing. **Dennis Chi:** Resources, Writing – review & editing. **Alexandra Snyder:** Conceptualization, Formal analysis, Funding acquisition, Investigation, Methodology, Writing – review & editing. **Travis J. Hollmann:** Conceptualization, Formal analysis, Funding acquisition, Investigation, Supervision, Resources, Validation, Methodology, Writing – review & editing. **Katherine L. Mager:** Conceptualization, Data curation, Supervision, Methodology, Writing – original draft, Writing – review & editing.

Declaration of Competing Interest

The authors declare that they have no known competing financial interests or personal relationships that could have appeared to influence the work reported in this paper.

Appendix A. Supplementary material

Supplementary data to this article can be found online at https://doi.org/10.1016/j.gore.2022.100926.

References

Barber, D.L., Wherry, E.J., Masopust, D., Zhu, B., Allison, J.P., Sharpe, A.H., Freeman, G. J., Ahmed, R., 2006. Restoring function in exhausted CD8 T cells during chronic viral infection. Nature 439 (7077), 682–687.

Blanc-Durand, F., Genestie, C., Galende, E.Y., Gouy, S., Morice, P., Pautier, P., Maulard, A., Mesnage, S., Le Formal, A., Brizais, C., Richardson, M., Leary, A., 2021. Distribution of novel immune-checkpoint targets in ovarian cancer tumor microenvironment: a dynamic landscape. Gynecol. Oncol. 160 (1), 279–284.

Bowtell, D.D., Böhm, S., Ahmed, A.A., Aspuria, P.-J., Bast, R.C., Beral, V., Berek, J.S., Birrer, M.J., Blagden, S., Bookman, M.A., Brenton, J.D., Chiappinelli, K.B., Martins, F.C., Coukos, G., Drapkin, R., Edmondson, R., Fotopoulou, C., Gabra, H., Galon, J., Gourley, C., Heong, V., Huntsman, D.G., Iwanicki, M., Karlan, B.Y., Kaye, A., Lengyel, E., Levine, D.A., Lu, K.H., McNeish, I.A., Menon, U., Narod, S.A., Nelson, B.H., Nephew, K.P., Pharoah, P., Powell, D.J., Ramos, P., Romero, I.L., Scott, C.L., Sood, A.K., Stronach, E.A., Balkwill, F.R., 2015. Rethinking ovarian cancer II: reducing mortality from high-grade serous ovarian cancer. Nat. Rev. Cancer 15 (11), 668–679.

Brunekreeft, K.L., Paijens, S.T., Wouters, M.C.A., Komdeur, F.L., Eggink, F.A., Lubbers, J. M., Workel, H.H., Van Der Slikke, E.C., Pröpper, N.E.J., Leffers, N., Adam, J., Pijper, H., Plat, A., Kol, A., Nijman, H.W., De Bruyn, M., 2020. Deep immune profiling of ovarian tumors identifies minimal MHC-I expression after neoadjuvant chemotherapy as negatively associated with T-cell-dependent outcome. Oncoimmunology 9 (1). https://doi.org/10.1080/2162402X.2020.1760705.

Center for Drug Evaluation, Research. Simultaneous review decisions for pembrolizumab plus lenvatinib in Aus [Internet]. 2019 [cited 2021 May 24]. Available from: <https://www.fda.gov/drugs/resources-information-approved-drugs/simultaneous-review-decisions-pembrolizumab-plus-lenvatinib-australia-canada-and-us>.

Davidson-Pilon, C., 2021. lifelines, survival analysis in Python. (cited 2021 Dec 5). Available from: <https://zenodo.org/record/5745573>.

Duan, Z., Luo, Y., 2021. Targeting macrophages in cancer immunotherapy. Sig. Transduct. Target Ther. 6 (1) https://doi.org/10.1038/s41392-021-00506-6.

Gubin, M.M., Esaulova, E., Ward, J.P., Malkova, O.N., Runci, D., Wong, P., Noguchi, T., Arthur, C.D., Meng, W., Alspach, E., Medrano, R.F.V., Fronick, C., Fehlings, M., Newell, E.W., Fulton, R.S., Sheehan, K.C.F., Oh, S.T., Schreiber, R.D., Artyomov, M. N., 2018. High-dimensional analysis delineates myeloid and lymphoid compartment remodeling during successful immune-checkpoint cancer therapy. Cell 175 (5), 1443. https://doi.org/10.1016/j.cell.2018.11.003.

Hamanishi, J., Mandai, M., Ikeda, T., Minami, M., Kawaguchi, A., Murayama, T., Kanai, M., Mori, Y., Matsumoto, S., Chikuma, S., Matsumura, N., Abiko, K., Baba, T., Yamaguchi, K., Ueda, A., Hosoe, Y., Morita, S., Yokode, M., Shimizu, A., Honjo, T., Konishi, I., 2015. Safety and antitumor activity of anti-PD-1 antibody, nivolumab, in patients with platinum-resistant ovarian cancer. J. Clin. Oncol. 33 (34), 4015–4022.

Jiménez-Sánchez, A., Cybulska, P., Mager, K.L., Koplev, S., Cast, O., Couturier, D.-L., Memon, D., Selenica, P., Nikolovski, I., Mazaheri, Y., Bykov, Y., Geyer, F.C., Macintyre, G., Gavarró, L.M., Drews, R.M., Gill, M.B., Papanastasiou, A.D., Sosa, R. E., Soslow, R.A., Walther, T., Shen, R., Chi, D.S., Park, K.J., Hollmann, T., Reis-Filho, J.S., Markowetz, F., Beltrao, P., Vargas, H.A., Zamarin, D., Brenton, J.D., Snyder, A., Weigelt, B., Sala, E., Miller, M.L., 2020. Unraveling tumor–immune heterogeneity in advanced ovarian cancer uncovers immunogenic effect of chemotherapy. Nat. Genet. 52 (6), 582–593.

Kalli, K.R., Oberg, A.L., Keeney, G.L., Christianson, T.J.H., Low, P.S., Knutson, K.L., Hartmann, L.C., 2008. Folate receptor alpha as a tumor target in epithelial ovarian cancer. Gynecol. Oncol. 108 (3), 619–626.

Ledermann, J.A., Colombo, N., Oza, A.M., Fujiwara, K., Birrer, M.J., Randall, L.M., Poddubskaya, E.V., Scambia, G., Shparyk, Y.V., Lim, M.C., Bhoola, S.M., Sohn, J., Yonemori, K., Stewart, R.A., Zhang, X., Zohren, F., Linn, C., Monk, B.J., 2020. Avelumab in combination with and/or following chemotherapy vs chemotherapy alone in patients with previously untreated epithelial ovarian cancer: results from the phase 3 javelin ovarian 100 trial. Gynecol. Oncol. 159, 13–14.

Makker, V., Rasco, D., Vogelzang, N.J., Brose, M.S., Cohn, A.L., Mier, J., Di Simone, C., Hyman, D.M., Stepan, D.E., Dutcus, C.E., Schmidt, E.V., Guo, M., Sachdev, P., Shumaker, R., Aghajanian, C., Taylor, M., 2019. Lenvatinib plus pembrolizumab in patients with advanced endometrial cancer: an interim analysis of a multicentre, open-label, single-arm, phase 2 trial. Lancet Oncol. 20 (5), 711–718.

Martin, U., Bock, D., Arseniev, L., Tornetta, M.A., Ames, R.S., Bautsch, W., et al., 1997. The human C3a receptor is expressed on neutrophils and monocytes, but not on B or T lymphocytes (Internet). J. Exp. Med. 186, 199–207. doi: 10.1084/jem.186.2.199.

Mellor, A.L., Munn, D.H., 2004. Ido expression by dendritic cells: tolerance and tryptophan catabolism. Nat. Rev. Immunol. 4 (10), 762–774.

Mesnage, S.J.L., Auguste, A., Genestie, C., Dunant, A., Pain, E., Drusch, F., Gouy, S., Morice, P., Bentivegna, E., Lhomme, C., Pautier, P., Michels, J., Le Formal, A., Cheaib, B., Adam, J., Leary, A.F., 2017. Neoadjuvant chemotherapy (NACT) increases immune infiltration and programmed death-ligand 1 (PD-L1) expression in epithelial ovarian cancer (EOC). Ann. Oncol. 28 (3), 651–657.

Moore, K.N., Oza, A.M., Colombo, N., Oaknin, A., Scambia, G., Lorusso, D., et al., 2021. Phase III, randomized trial of mirvetuximab soravtansine versus chemotherapy in patients with platinum-resistant ovarian cancer: primary analysis of FORWARD I. Ann Oncol. 32 (6), 757–765.

Nowak, M., Klink, M., 2020. The role of tumor-associated macrophages in the progression and chemoresistance of ovarian cancer. Cells (Internet) 9 (5). doi: 10.3390/cells9051299.

O'Malley, D.M., Matulonis, U.A., Birrer, M.J., Castro, C.M., Gilbert, L., Vergote, I., Martin, L.P., Mantia-Smaldone, G.M., Martin, A.G., Bratos, R., Penson, R.T., Malek, K., Moore, K.N., 2020. Phase Ib study of mirvetuximab soravtansine, a folate receptor alpha (FRα)-targeting antibody-drug conjugate (ADC), in combination with bevacizumab in patients with platinum-resistant ovarian cancer. Gynecol Oncol. 157 (2), 379–385.

Ovarian Tumor Tissue Analysis (OTTA) Consortium, Goode, E.L., Block, M.S., Kalli, K.R., Vierkant, R.A., Chen, W., et al., 2017. Dose-response association of CD8+ tumor-infiltrating lymphocytes and survival time in high-grade serous ovarian cancer. JAMA Oncol. 3 (12), e173290.

Shevach, E.M., Stephens, G.L., 2006. The GITR-GITRL interaction: co-stimulation or contrasuppression of regulatory activity? Nat. Rev. Immunol. 6 (8), 613–618.

Sun, N.-Y., Chen, Y.-L., Wu, W.-Y., Lin, H.-W., Chiang, Y.-C., Chang, C.-F., et al., 2019. Blockade of PD-L1 enhances cancer immunotherapy by regulating dendritic cell maturation and macrophage polarization. Cancers (Internet) 11 (9). doi: 10.3390/cancers11091400.

Varga, A., Piha-Paul, S.A., Ott, P.A., Mehnert, J.M., Berton-Rigaud, D., Johnson, E.A., Cheng, J.D., Yuan, S., Rubin, E.H., Matei, D.E., 2015. Antitumor activity and safety of pembrolizumab in patients (pts) with PD-L1 positive advanced ovarian cancer: Interim results from a phase Ib study. JCO 33 (15_suppl), 5510.

Verhaak, R.G.W., Tamayo, P., Yang, J.-Y., Hubbard, D., Zhang, H., Creighton, C.J., et al., 2013. Prognostically relevant gene signatures of high-grade serous ovarian carcinoma. J. Clin. Invest. 123 (1), 517–525.

Wang, Y., Zhang, H., He, Y.-W., 2019 Jul. The complement receptors C3aR and C5aR are a new class of immune checkpoint receptor in cancer immunotherapy. Front Immunol. 19 (10), 1574.

Zamarin, D., Burger, R.A., Sill, M.W., Powell, D.J., Lankes, H.A., Feldman, M.D., Zivanovic, O., Gunderson, C., Ko, E., Mathews, C., Sharma, S., Hagemann, A.R., Khleif, S., Aghajanian, C., 2020. Randomized phase II trial of nivolumab versus nivolumab and ipilimumab for recurrent or persistent ovarian cancer: an NRG oncology study. JCO 38 (16), 1814–1823.

Zamarin, D., Walderich, S., Holland, A., Zhou, Q., Iasonos, A.E., Torrisi, J.M., et al., 2020. Safety, immunogenicity, and clinical efficacy of durvalumab in combination with folate receptor alpha vaccine TPIV200 in patients with advanced ovarian cancer: a phase II trial. J. Immunother. Cancer (Internet). doi: 10.1136/jitc-2020-000829.

Zhang, L., Conejo-Garcia, J.R., Katsaros, D., Gimotty, P.A., Massobrio, M., Regnani, G., Makrigiannakis, A., Gray, H., Schlienger, K., Liebman, M.N., Rubin, S.C., Coukos, G., 2003. Intratumoral T cells, recurrence, and survival in epithelial ovarian cancer. N Engl J Med. 348 (3), 203–213.